Letter

Near-field radiation in BAs and BSb dominated by four-phonon scattering

Dudong Feng,[*] Xiaolong Yang,[*,†] Zherui Han, and Xiulin Ruan[‡]
School of Mechanical Engineering and the Birck Nanotechnology Center, Purdue University, West Lafayette, Indiana 47907-2088, USA

(Received 3 January 2023; revised 23 January 2024; accepted 2 February 2024; published 29 February 2024)

Inelastic scattering processes typically introduce friction among carriers and reduce the transport properties of photons, phonons, and electrons. However, we predict that in contrast to the role in reducing thermal conductivity, four-phonon scattering dominates the near-field radiative heat transfer (NFRHT) in both boron arsenide (BAs) and boron antimonide. Including four-phonon scattering results in a nearly 400-fold increase in the total heat flux between two BAs thin films compared to three-phonon scattering alone. This nonintuitive enhancement arises from the large number of NFRHT channels activated by four-phonon scattering, outcompeting the effect of decreased coupling strength of surface phonon polaritons at the resonance frequency. Additionally, we point out that four-phonon scattering decreases NFRHT in certain other systems.

DOI: 10.1103/PhysRevB.109.L081409

Enabled by coupled surface phonon polaritons (SPhPs) at nanoscales, near-field thermal radiation between polar dielectrics achieves an orders of magnitude enhancement beyond the blackbody limit governed by Planck's law [1–3]. Such super-Planckian thermal radiation has been demonstrated experimentally [2–4], leading to the developments of energy harvesting [5–8], thermal management [9] and modulation [10,11], and near-field imaging and sensing [12–14].

As hybrid quasiparticles are formed by the strong coupling of surface electromagnetic (EM) modes and localized optical phonons, the phonon nature of SPhPs has been little investigated in the scenario of near-field radiative heat transfer (NFRHT) [11]. Revealed by the dispersion relation, SPhPs can only be excited within the reststrahlen band, which is bounded by the frequency of the zone-center transverse optical (TO), ω_{TO}, and longitudinal optical (LO) phonon modes, ω_{LO}. The dielectric function at this range can be effectively described by the Lorentz oscillator model, and the damping factor is the phonon linewidth, which manifests the phonon anharmonicity of the infrared (IR) active phonon at the zone center [15]. According to fluctuational electrodynamics, the coupling strength of SPhPs is characterized by the damping factor, which explicitly connects the near-field radiative heat flux with phonon scattering processes.

While the lowest-order theory of phonon-phonon scattering was historically sufficient for explaining material anharmonicity [16,17], considering higher-order intrinsic scattering, particularly four-phonon scattering, has significantly improved agreement between theoretical predictions and experimental measurements recently. Boron arsenide (BAs) was predicted to exhibit a high thermal conductivity of 2200 W/m K due to weak three-phonon scattering [16]. Later, a general theory of four-phonon scattering was introduced [18], predicting a reduced thermal conductivity of 1400 W/m K for BAs at room temperature [19]. This significant reduction is due to restricted three-phonon scattering space making four-phonon scattering relatively large. Three subsequent experiments confirmed BAs thermal conductivities of 1000–1300 W/m K [20–22]. BAs has also drawn significant attention for its high bipolar mobilities, which were first predicted [23] and later experimentally confirmed [24,25]. Besides thermal conductivity, four-phonon scattering was recently shown to be significant in IR [15,26] and Raman spectra [27] of many materials, by resolving previous experiment-theory discrepancies for these materials. While extensive studies have delved into the influence of four-phonon scattering on related properties of polar materials [15,28,29], its impact on NFRHT remains unexplored.

In this Letter, we predict that four-phonon scattering can have a dominant contribution to NFRHT over three-phonon scattering in two prototype polar materials: BAs and boron antimonide (BSb). By combining first-principles calculations and fluctuational electrodynamics, we quantitatively bridge the near-field radiative heat flux and anharmonic phonon scattering. While the inclusion of higher-order phonon scattering processes was known to result in more friction among phonons and reduce thermal conductivity, here we reveal, surprisingly, that four-phonon scattering is favorable to NFRHT between polar dielectric slabs and leads to a 300-fold enhancement to the total heat flux for BAs and a fourfold enhancement to that for BSb. By varying temperatures and gap distances, we show that a smaller vacuum gap distance and lower-temperature difference can make four-phonon scattering more dominant on the radiative heat transfer over three-phonon scattering. Meanwhile, considering the existence of optimum damping factor for NFRHT, we point out the possibility of four-phonon scattering to decrease NFRHT in certain other systems. Our work could open an avenue of phonon engineering and materials screening for near-field thermal modulation and management.

We start with the calculation of the temperature-dependent damping factor, which is equal to the IR-active phonon

[*]These authors contributed equally to this work.
[†]Present address: College of Physics, and Center of Quantum Materials and Devices, Chongqing University, Chongqing 401331, China.
[‡]ruan@purdue.edu

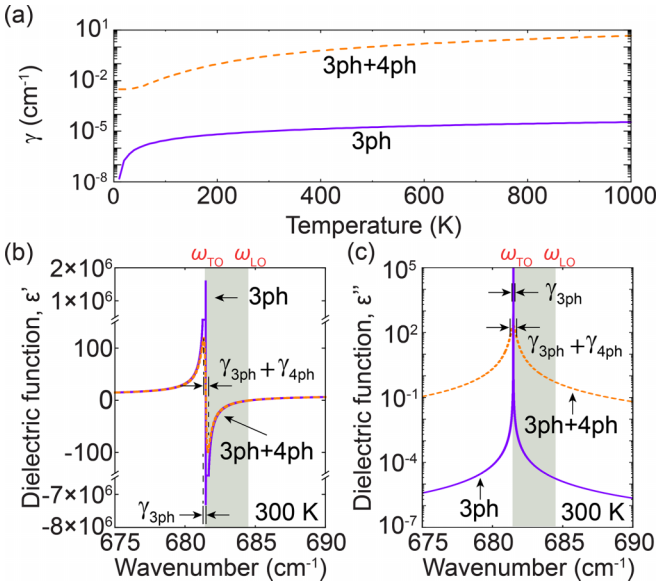

FIG. 1. (a) The damping factors of isotopically pure BAs as a function of temperature with or without γ_{4ph} [15]. (b) The real and (c) imaginary parts of the dielectric function of isotopically pure BAs with or without γ_{4ph} at 300 K. The shaded area is the reststrahlen band.

linewidth, by summing its three-and four-phonon scattering rates with other phonons in the first Brillouin zone within density functional perturbation theory in the Supplemental Material [30] (see also Refs. [31–38] therein),

$$\gamma(T) = \gamma_{3ph}(T) + \gamma_{4ph}(T), \tag{1}$$

where T is the material temperature at thermal equilibrium, and γ represents the damping factor. The subscripts 3ph and 4ph indicate the contributions from three-phonon and four-phonon scattering, respectively. Here, we consider isotope pure BAs for simplicity, hence no phonon isotope scattering is needed. Figure 1(a) shows the temperature-dependent damping factors of BAs before and after including four-phonon scattering. Although a monotonically increasing trend is shown as temperature increases with or without four-phonon scattering, the damping factor due to four-phonon scattering is four to six orders of magnitude larger than that due to three-phonon scattering. To satisfy the energy and momentum conservation in a phonon scattering process, three-phonon scattering, especially the process involving two acoustic phonons and one optical phonon (aao), is largely suppressed due to the large a-o gap so that γ_{3ph} is only 10^{-5} cm^{-1} at 300 K, while γ_{4ph} can reach 0.29 cm^{-1}. Therefore, four-phonon scattering dominates the damping force on the hypothetical optical oscillator used in the Lorentz oscillator model of the dielectric function,

$$\epsilon(\omega) = \epsilon_\infty\left(1 + \frac{\omega_{LO}^2 - \omega_{TO}^2}{\omega_{TO}^2 - \omega^2 - i\omega\gamma}\right), \tag{2}$$

where $\epsilon_\infty = 9.83$ represents the dielectric constant at the high-frequency limit, and ω is the angular frequency. Here, we use the unit of wave number in the Lorentz model. $\omega_{TO} = 681.5$ cm^{-1} and $\omega_{LO} = 684.7$ cm^{-1}. The phonon frequencies and damping factors, obtained from first-principles calculations, are detailed in the Supplemental Material [30].

The dielectric functions of BAs are calculated with or without four-phonon scattering at 300 K, and the real (ϵ') and imaginary parts (ϵ'') of the dielectric functions around the reststrahlen band are shown in Figs. 1(b) and 1(c), respectively. We can clearly observe a strong oscillation of ϵ' around ω_{TO}, when $\epsilon'(\omega_{TO}) = \epsilon_\infty$ in Fig. 1(b) [2]. The peak value of ϵ' without four-phonon scattering is four orders of magnitude larger than that with four-phonon scattering. The spectral width between the peak and valley values of ϵ' is equivalent to the damping factor. As the four-phonon scattering process dominates the anharmonic phonon scattering in BAs, this spectral width of ϵ' of $\gamma_{3ph} + \gamma_{4ph}$ is much larger than that of γ_{3ph}. As we can see from Fig. 1(c), at the frequency far away from ω_{TO}, ϵ'' is negligible, which indicates that the absorption is only appreciable within an interval of the damping factor around ω_{TO} [2]. The full width at the half maximum (FWHM) of this absorption spectrum is equal to the corresponding damping factor with or without four-phonon scattering included. Although ϵ'' including four-phonon scattering has a wider FWHM, its peak value is much lower than that without including four-phonon scattering. This trade-off phenomenon implies, when the damping factor increases, more lattice vibration modes can potentially assist the light-matter interaction around ω_{TO}, while the resonance strength is much suppressed. However, we observe a negative ϵ' and a large ϵ'' within the reststralen band, where the normal reflectivity can reach close to unity due to the near-zero refractive index (n) and large extinction coefficient (κ), i.e., the complex refractive index is almost pure imaginary [15]. Therefore, the polar materials are highly reflecting when interacting with propagating waves (far field), while interacting with evanescent waves (near field), especially surface waves, the materials become highly absorbing due to the phonon tunneling effect.

We first present the spectral heat fluxes (q_ω) with three different damping factors in Fig. 2(a). A fluctuational electrodynamics formalism is applied to characterize NFRHT, as detailed in the Supplemental Material [30]. A near-field radiation system composed of two bulk BAs with a hypothetical damping factor, $\gamma = 0$, is calculated as the baseline, where the result indicates that the radiative heat transfer is completely prohibited within the reststrahlen band. Since $n = 0$, a perfect polar dielectric is perfectly reflecting so that propagating waves are fully confined within BAs bulks. Additionally, the excitation of coupled SPhPs to transfer energy requires a nonzero damping factor based on the analysis of the local photon density of states [30]. In other words, no exchange of photons of any mode can occur between two perfect polar dielectric bulks, and phonon anharmonicity is necessary to facilitate the NFRHT mediated by SPhPs. To explicitly examine the four-phonon scattering effect on NFRHT, we compare q_ω with or without γ_{4ph}. Within the reststrahlen band, q_ω with γ_{3ph} is mostly four to siz orders of magnitude smaller than that with $\gamma_{3ph} + \gamma_{4ph}$. The wider FWHM of q_ω with $\gamma_{3ph} + \gamma_{4ph}$ comparing to that with γ_{3ph} indicates that more optical phonon modes can participate in NFRHT through phonon scattering when four-phonon scattering is included. As $q_\omega \sim \mathrm{Im}(\epsilon_1)\mathrm{Im}(\epsilon_2)/|(\epsilon_1+1)(\epsilon_2+1)|^2$, the peak value of q_ω occurs at the resonant frequency (ω_{res}) when $\epsilon_1 = -1$ or

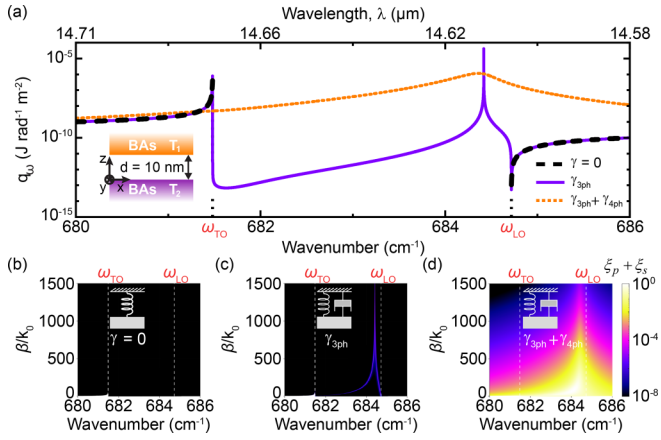

FIG. 2. (a) The spectral heat fluxes between two BAs bulks with three different damping factors. The contour plots of the energy transmission coefficient ($\xi_s + \xi_p$) between two BAs bulks with (b) $\gamma = 0$, (c) γ_{3ph}, and (d) $\gamma_{3ph} + \gamma_{4ph}$. A mass-spring-damper system visualizes the Lorentz oscillations of the bonded crystals. With $\gamma = 0$, the mass-spring-damper system can be simplified as a mass-spring system. When $\gamma \neq 0$, the damper has a corresponding damping coefficient with or without γ_{4ph}. The energy transmission coefficient is calculated with respect to the normalized parallel wave vector β/k_0 and angular frequency, with $k_0 = \omega/c$ (ω is the wave vector at vacuum, and c is the speed of light). The inset plot in (a) indicates the configuration of the near-field radiation system with a 10 nm vacuum gap spacing and the temperatures of two BAs are set as $T_1 = 1000$ K and $T_2 = 300$ K, respectively. The vacuum gap distance is the default in this Letter unless stated otherwise.

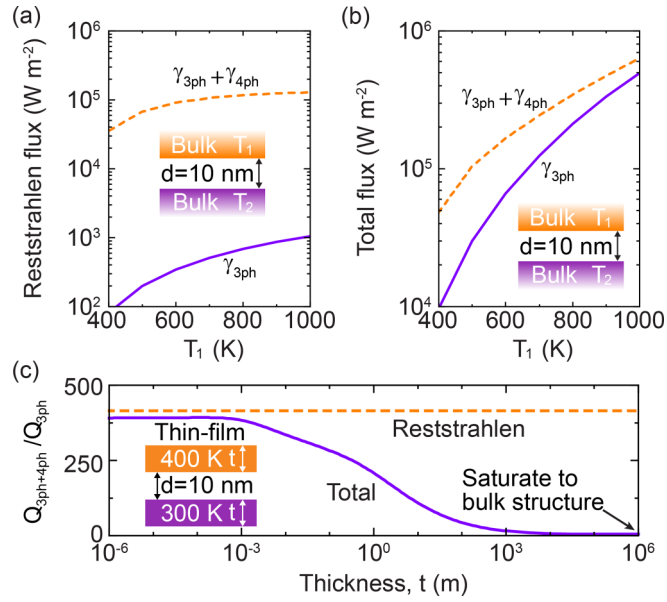

FIG. 3. (a) The reststrahlen band and (b) the total heat flux with or without considering four-phonon scattering with respect to T_1. Note that $T_2 = 300$ K. (c) The effect of four-phonon scattering on NFRHT with respect to the thicknesses of BAs films.

$\epsilon_2 = -1$. q_ω at ω_{TO} with $\gamma = 0$ or γ_{3ph} is much higher than that with $\gamma_{3ph} + \gamma_{4ph}$, because $n(\omega_{TO})$ with $\gamma = 0$ or γ_{3ph} is much larger than that with $\gamma_{3ph} + \gamma_{4ph}$. Therefore, more frustrated modes can tunnel through the vacuum gap and enhance NFRHT. The same reason can be applied to explain q_ω at ω_{LO}.

To investigate the contribution of each electromagnetic mode, we calculate the energy transmission coefficient (ξ) as a function of the normalized parallel wave vector and the angular frequency for different damping factors, as shown in Figs. 2(b)–2(d) for BAs. The calculation of ξ and results of BSb can be found in the Supplemental Material [30]. Each point on the contour plot represents a channel for radiative heat transfer at a specific parallel wave vector and angular frequency. The brighter color represents a higher photon transmission probability at this channel. As shown in Fig. 2(b), we can clearly see that neither a coupled evanescent wave nor propagating waves supports radiative heat transfer within the reststrahlen band when $\gamma = 0$. As indicated by the mass-spring system, no scattering acts as the friction force so that the surface resonance can never be excited through other photon modes at different frequencies. Moreover, as no local photon density of states supports the propagating waves [30], the radiative heat transfer is completely forbidden within the reststrahlen band. Outside the reststrahlen band, heat can be transferred by propagating modes and frustrated modes, and no surface modes can be excited to support radiative heat transfer because the permittivity is not negative. As the damping factor only including three-phonon scattering is extremely small, the energy transmission coefficient is only significant along the dispersion relation of coupled SPhPs [30]. The peak value of q_ω with γ_{3ph} at ω_{res} in Fig. 2(a) arises from the surface modes excited at the parallel wave vector close to $1500k_0$. Comparing between Figs. 2(c) and 2(d), the coupled SPhPs are widely and strongly excited when four-phonon scattering is considered in the damping factor. As the damping force of $\gamma_{3ph} + \gamma_{4ph}$ is much larger than that of γ_{3ph}, the Lorentz oscillator with $\gamma_{3ph} + \gamma_{4ph}$ can interact with more modes at various frequencies so that more channels are activated to support the coupled SPhPs. Nonetheless, q_ω at ω_{res} is dominated by the surface modes with large parallel wave vectors but the overall radiative heat transfer is enhanced when four-phonon scattering is involved. Therefore, NFRHT between two bulk BAs at the nanoscale is enabled by phonon anharmonicity and greatly contributed by four-phonon scattering.

To examine the four-phonon scattering effect on NFRHT, we calculate the heat flux of the reststrahlen band (Q_{Rest}) and the total heat flux (Q_t) for hot side temperatures ranging from 400 to 1000 K. As shown in Fig. 3(a), Q_{Rest} monotonically increases with respect to T_1. Q_{Rest} with four-phonon scattering is nearly 500 times higher than that with only three-phonon scattering when $T_1 = 400$ K, while this enhancement reduces to 100 times when $T_1 = 1000$ K. Although a higher temperature indicates a larger damping factor, more scattering processes do not necessarily enhance NFRHT linearly. The trade-off between the resonance peak value and the FWHM of the spectral heat flux implies that an optimal pair of damping factors may exist. The same trend of Q_t with respect to T_1 is also observed in Fig. 3(b), while the enhancement brought by four-phonon scattering become much smaller, since the coupled SPhPs only contribute a fraction to the total radiative heat transfer. The enhancement due to four-phonon scattering decreases from 5 times to 1.3 times when T_1 increases from 400 to 1000 K, driven by the closer agreement of $\gamma_{3ph} + \gamma_{4ph}$ at 400 K

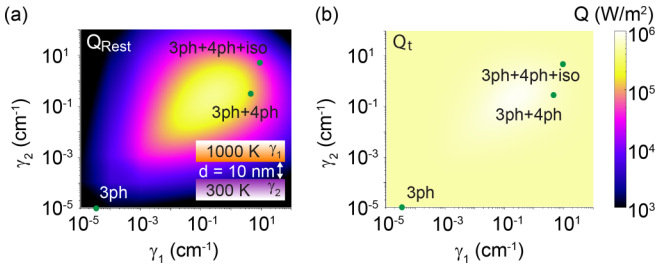

FIG. 4. The contour plot of the reststrahlen band (a) and the total heat flux (b) with respect to the artificially tuned damping factors. Three specific points are marked to represent actual situations when three-phonon scattering, four-phonon scattering, and phonon-isotope scattering are each added into the consideration.

with the value at 300 K, facilitating better coupling of the surface modes. Furthermore, the effect of four-phonon scattering becomes more apparent when reducing the thickness of the polar dielectric. To quantify this effect, we define a ratio R_{4ph} as $Q_{3ph+4ph}/Q_{3ph}$ for both total heat flux and reststrahlen band flux. As shown Fig. 3(c), the maximum R_{4ph} of total heat flux can surpass 300 since the radiative heat flux carried by propagating waves is suppressed in thin-film structures. Consequently, at small thicknesses, the ratio of the total heat flux closely matches that of the reststrahlen band flux. However, as the thickness increases, the ratio of the total heat flux saturates and approaches the value observed in the semi-infinite bulk structure [Figs. 3(a) and 3(b)]. A similar analysis and conclusions can be drawn for BSb [30]. Moreover, the significance of four-phonon scattering on NFRHT is investigated from the near- to far-field regime in the Supplemental Material [30].

We also perform a parametric sweep on the arbitrarily tuned damping factors of two BAs bulks at 1000 and 300 K, and create two contour plots (Fig. 4) of Q_{Rest} and Q_t to reveal the direct relation between phonon anharmonicity and radiative heat transfer. We mark three specific points representing the situations when considering 3ph, 3ph+4ph, and 3ph+4ph+iso, respectively. Clearly, there exist maximum values of both Q_{Rest} and Q_t, and the corresponding damping factors of the hot and cold sides are both 0.21 cm^{-1}, which are at the order of 10% of TO-LO splitting [39,40]. When the damping factors are different for the hot and cold sides, the activated number of NFRHT channels is determined mostly by the smaller value of γ_1 and γ_2 due to the coupling effect of SPhPs, and the coupling strength of each channel is restricted by the larger value between the two damping factors. A pair of small damping factors indicate a narrow-band spectral heat flux but with a large peak at the resonant frequency. Therefore, as the pair of damping factors increases from 10^{-5} cm^{-1} to the optimal values, the peak spectral heat flux reduces but more SPhPs are coupled around ω_{res} and Q_{Rest} increases. Q_{Rest} becomes more significant in radiative heat transfer, leading to a maximum in Q_t. Once the pair of damping factors passes the optimal values, the resonant effect of coupled SPhPs becomes weaker and less radiative heat flux is carried by the surface modes. The three specific points representing the actual cases indicate that including four-phonon scattering can greatly enhance the radiative heat transfer processes, while further including the isotope effect is likely to deteriorate NFRHT of BAs. However, isotope engineering has been shown to effectively tune radiative heat transfer [41]. With a recent estimate of fifth-order or even higher-order phonon scatterings [42], the residue damping factor results from these phonon scatterings can potentially modify radiative heat transfer for both the far- and near-field regimes. The enhancement or deterioration of NFRTHT due to higher-order phonon scattering in different materials depends on whether γ_{4ph} can drive the damping factor towards the optimal value or away from it. Normally, four-phonon scattering can dominate NFRHT in materials where the three-phonon scattering is greatly suppressed. Conversely, if a material's three-phonon scattering rate is already near or at the optimum, adding four-phonon scattering may drive the total scattering rate past the optimum, hence reducing NFRHT. Nevertheless, the nonmonotonic dependence of NFRHT on phonon scattering rates is distinctive from thermal conductivity where small phonon scattering rates are always required to increase the thermal conductivity for BAs and BSb.

In conclusion, we have quantitatively established that phonon anharmonicity is crucial for SPhPs-mediated radiative heat transfer. By considering four-phonon scattering alongside three-phonon scattering, we observe a remarkable enhancement of the total heat flux between BAs bulks by over two orders of magnitude, in contrast to its role in reducing thermal conductivity. The impact of four-phonon scattering on NFRHT becomes more pronounced with smaller vacuum gap distances and film thicknesses for both BAs and BSb. Moreover, through artificial tuning of the damping factor in BAs, we identify an optimal pair of damping factors that maximize radiative heat flux, indicating that the enhancement of NFRHT through four-phonon scattering requires materials with a suppressed damping factor due to three-phonon scattering. Therefore, we also suggest that four-phonon scattering decreases NFRHT in certain other systems. Our work not only unveils the relationship between phonon scattering and NFRHT in polar dielectrics, highlighting the potential of phonon engineering to control radiative heat transfer at nanoscales, this study also opens a promising avenue for near-field thermal regulation and management techniques.

D.F. and X.R. acknowledge partial support from the U.S. National Science Foundation through Award No. 2102645. Z.H. and X.R. acknowledge partial support from the U.S. National Science Foundation through Award No. 2015946.

[1] J.-P. Mulet, K. Joulain, R. Carminati, and J.-J. Greffet, Enhanced radiative heat transfer at nanometric distances, Microscale Thermophys. Eng. **6**, 209 (2002).

[2] Z. M. Zhang, *Nano/Microscale Heat Transfer* (Springer, Cham, 2020).

[3] S. Shen, A. Narayanaswamy, and G. Chen, Surface phonon polaritons mediated energy transfer between nanoscale gaps, Nano Lett. **9**, 2909 (2009).

[4] M. Ghashami, H. Geng, T. Kim, N. Iacopino, S. K. Cho, and K. Park, Precision measurement of phonon-polaritonic near-field

energy transfer between macroscale planar structures under large thermal gradients, Phys. Rev. Lett. **120**, 175901 (2018).

[5] D. Feng, Study of the photon checmical potential in semicondcutor radiative energy converters at micro/nanoscales, Ph.D. thesis, Georgia Institute of Technology, 2021.

[6] A. Narayanaswamy and G. Chen, Surface modes for near field thermophotovoltaics, Appl. Phys. Lett. **82**, 3544 (2003).

[7] D. Feng, S. K. Yee, and Z. M. Zhang, Improved performance of a near-field thermophotovoltaic device by a back gapped reflector, Sol. Energy Mater. Sol. Cells **237**, 111562 (2022).

[8] D. Feng, X. Ruan, S. K. Yee, and Z. M. Zhang, Thermoradiative devices enabled by hyperbolic phonon polaritons at nanoscales, Nano Energy **103**, 107831 (2022).

[9] A. Principi, M. B. Lundeberg, N. C. H. Hesp, K.-J. Tielrooij, F. H. L. Koppens, and M. Polini, Super-Planckian electron cooling in a van der Waals stack, Phys. Rev. Lett. **118**, 126804 (2017).

[10] D. Feng, S. K. Yee, and Z. M. Zhang, Near-field photonic thermal diode based on hBN and InSb films, Appl. Phys. Lett. **119**, 181111 (2021).

[11] C. R. Otey, W. T. Lau, and S. Fan, Thermal rectification through vacuum, Phys. Rev. Lett. **104**, 154301 (2010).

[12] J. D. Caldwell, L. Lindsay, V. Giannini, I. Vurgaftman, T. L. Reinecke, S. A. Maier, and O. J. Glembocki, Low-loss, infrared and terahertz nanophotonics using surface phonon polaritons, Nanophotonics **4**, 44 (2015).

[13] J.-J. Greffet, R. Carminati, K. Joulain, J.-P. Mulet, S. Mainguy, and Y. Chen, Coherent emission of light by thermal sources, Nature (London) **416**, 61 (2002).

[14] R. Hillenbrand, T. Taubner, and F. Keilmann, Phonon-enhanced light–matter interaction at the nanometre scale, Nature (London) **418**, 159 (2002).

[15] X. Yang, T. Feng, J. S. Kang, Y. Hu, J. Li, and X. Ruan, Observation of strong higher-order lattice anharmonicity in Raman and infrared spectra, Phys. Rev. B **101**, 161202(R) (2020).

[16] L. Lindsay, D. A. Broido, and T. L. Reinecke, First-principles determination of ultrahigh thermal conductivity of boron arsenide: A competitor for diamond? Phys. Rev. Lett. **111**, 025901 (2013).

[17] D. A. Broido, M. Malorny, G. Birner, N. Mingo, and D. A. Stewart, Intrinsic lattice thermal conductivity of semiconductors from first principles, Appl. Phys. Lett. **91**, 231922 (2007).

[18] T. Feng and X. Ruan, Quantum mechanical prediction of four-phonon scattering rates and reduced thermal conductivity of solids, Phys. Rev. B **93**, 045202 (2016).

[19] T. Feng, L. Lindsay, and X. Ruan, Four-phonon scattering significantly reduces intrinsic thermal conductivity of solids, Phys. Rev. B **96**, 161201(R) (2017).

[20] F. Tian, B. Song, X. Chen, N. K. Ravichandran, Y. Lv, K. Chen, S. Sullivan, J. Kim, Y. Zhou, T.-H. Liu, M. Goni, Z. Ding, J. Sun, G. A. G. U. Gamage, H. Sun, H. Ziyaee, S. Huyan, L. Deng, J. Zhou, A. J. Schmidt *et al.*, Unusual high thermal conductivity in boron arsenide bulk crystals, Science **361**, 582 (2018).

[21] J. S. Kang, M. Li, H. Wu, H. Nguyen, and Y. Hu, Experimental observation of high thermal conductivity in boron arsenide, Science **361**, 575 (2018).

[22] S. Li, Q. Zheng, Y. Lv, X. Liu, X. Wang, P. Y. Huang, D. G. Cahill, and B. Lv, High thermal conductivity in cubic boron arsenide crystals, Science **361**, 579 (2018).

[23] T.-H. Liu, B. Song, L. Meroueh, Z. Ding, Q. Song, J. Zhou, M. Li, and G. Chen, Simultaneously high electron and hole mobilities in cubic boron-V compounds: BP, BAs, and BSb, Phys. Rev. B **98**, 081203(R) (2018).

[24] J. Shin, G. A. Gamage, Z. Ding, K. Chen, F. Tian, X. Qian, J. Zhou, H. Lee, J. Zhou, L. Shi, T. Nguyen, F. Han, M. Li, D. Broido, A. Schmidt, Z. Ren, and G. Chen, High ambipolar mobility in cubic boron arsenide, Science **377**, 437 (2022).

[25] S. Yue, F. Tian, X. Sui, M. Mohebinia, X. Wu, T. Tong, Z. Wang, B. Wu, Q. Zhang, Z. Ren, J. Bao, and X. Liu, High ambipolar mobility in cubic boron arsenide revealed by transient reflectivity microscopy, Science **377**, 433 (2022).

[26] Z. Tong, X. Yang, T. Feng, H. Bao, and X. Ruan, First-principles predictions of temperature-dependent infrared dielectric function of polar materials by including four-phonon scattering and phonon frequency shift, Phys. Rev. B **101**, 125416 (2020).

[27] Z. Han, X. Yang, S. E. Sullivan, T. Feng, L. Shi, W. Li, and X. Ruan, Raman linewidth contributions from four-phonon and electron-phonon interactions in graphene, Phys. Rev. Lett. **128**, 045901 (2022).

[28] N. K. Ravichandran and D. Broido, Phonon-phonon interactions in strongly bonded solids: Selection rules and higher-order processes, Phys. Rev. X **10**, 021063 (2020).

[29] Y. Xia, V. I. Hegde, K. Pal, X. Hua, D. Gaines, S. Patel, J. He, M. Aykol, and C. Wolverton, High-throughput study of lattice thermal conductivity in binary rocksalt and zinc blende compounds including higher-order anharmonicity, Phys. Rev. X **10**, 041029 (2020).

[30] See Supplemental Material at http://link.aps.org/supplemental/10.1103/PhysRevB.109.L081409 for computational details and extra results.

[31] B. Song, A. Fiorino, E. Meyhofer, and P. Reddy, Near-field radiative thermal transport: From theory to experiment, AIP Adv. **5**, 053503 (2015).

[32] G. Kresse and J. Furthmüller, Efficiency of *ab-initio* total energy calculations for metals and semiconductors using a plane-wave basis set, Comput. Mater. Sci. **6**, 15 (1996).

[33] G. Kresse and J. Hafner, *Ab initio* molecular dynamics for liquid metals, Phys. Rev. B **47**, 558 (1993).

[34] J. P. Perdew, K. Burke, and M. Ernzerhof, Generalized gradient approximation made simple, Phys. Rev. Lett. **77**, 3865 (1996).

[35] A. Togo, F. Oba, and I. Tanaka, First-principles calculations of the ferroelastic transition between rutile-type and $CaCl_2$-type SiO_2 at high pressures, Phys. Rev. B **78**, 134106 (2008).

[36] W. Li, J. Carrete, N. A. Katcho, and N. Mingo, ShengBTE: A solver of the Boltzmann transport equation for phonons, Comput. Phys. Commun. **185**, 1747 (2014).

[37] Z. Han, X. Yang, W. Li, T. Feng, and X. Ruan, Four-phonon: An extension module to ShengBTE for computing four-phonon scattering rates and thermal conductivity, Comput. Phys. Commun. **270**, 108179 (2022).

[38] S. Basu and Z. M. Zhang, Maximum energy transfer in near-field thermal radiation at nanometer distances, J. Appl. Phys. **105**, 093535 (2009).

[39] R. Mittapally, J. W. Lim, L. Zhang, O. D. Miller, P. Reddy, and E. Meyhofer, Probing the limits to near-field heat transfer

enhancements in phonon-polaritonic materials, Nano Lett. **23**, 2187 (2023).

[40] X. J. Wang, S. Basu, and Z. M. Zhang, Parametric optimization of dielectric functions for maximizing nanoscale radiative transfer, J. Phys. D: Appl. Phys. **42**, 245403 (2009).

[41] L. Xie and B. Song, Isotope effect on radiative thermal transport, Phys. Rev. B **107**, 134308 (2023).

[42] X. Yang, T. Feng, J. Li, and X. Ruan, Evidence of fifth- and higher-order phonon scattering entropy of zone-center optical phonons, Phys. Rev. B **105**, 115205 (2022).